

Lawrence Berkeley National Laboratory

Recent Work

Title

Cross-section Transmission Electron Microscopy Study of Carbon Implanted Layers in Silicon

Permalink

<https://escholarship.org/uc/item/8hg934bm>

Authors

Wong, H.

Lou, J.

Cheung, N.W.

Publication Date

1990-03-25



Lawrence Berkeley Laboratory

UNIVERSITY OF CALIFORNIA

Materials & Chemical Sciences Division

Submitted to Applied Physics Letters

Cross-section Transmission Electron Microscopy Study of Carbon Implanted Layers in Silicon

H. Wong, J. Lou, and N.W. Cheung

March 1990



Prepared for the U.S. Department of Energy under Contract Number DE-AC03-76SF00098.

1 LOAN COPY 1
1 Circulates 1
1 For 2 weeks 1

Bldg. 50 Library.

LBL-28794

Copy 2

DISCLAIMER

This document was prepared as an account of work sponsored by the United States Government. While this document is believed to contain correct information, neither the United States Government nor any agency thereof, nor the Regents of the University of California, nor any of their employees, makes any warranty, express or implied, or assumes any legal responsibility for the accuracy, completeness, or usefulness of any information, apparatus, product, or process disclosed, or represents that its use would not infringe privately owned rights. Reference herein to any specific commercial product, process, or service by its trade name, trademark, manufacturer, or otherwise, does not necessarily constitute or imply its endorsement, recommendation, or favoring by the United States Government or any agency thereof, or the Regents of the University of California. The views and opinions of authors expressed herein do not necessarily state or reflect those of the United States Government or any agency thereof or the Regents of the University of California.

**CROSS-SECTION TRANSMISSION ELECTRON MICROSCOPY
STUDY OF CARBON-IMPLANTED LAYERS IN SILICON**

H. Wong, J. Lou, and N.W. Cheung

University of California,
Dept. of EECS, Berkeley, CA. 94720

E.P. Kvam, K.M. Yu, D.A. Olson, and J. Washburn

Materials and Chemical Sciences Division
Lawrence Berkeley Laboratory
Berkeley, CA. 94720

This work was supported in part, by California State MICRO program, and by the Director, Office of Energy Research, Office of Basic Energy Sciences, Materials Science Division of the U.S. Department of Energy under Contract No. DE-AC03-76SF00098.

Cross-section Transmission Electron Microscopy Study of Carbon Implanted Layers in Silicon

H. Wong, J. Lou, and N.W. Cheung

Dept. of EECS, University of California, Berkeley, CA 94720

E.P. Kvam, K.M. Yu, D.A. Olson, and J. Washburn

Materials & Chemical Sciences Division

Lawrence Berkeley Laboratory and University of California, Berkeley, CA 94720

Abstract

We have used cross-section transmission electron microscopy (XTEM) to study microstructures of carbon-implanted silicon layers after high temperature annealing. It was found that the threshold dose for extended defect formation was much higher for carbon implantation than for other ion species such as B, P, and O. In 2.4 MeV carbon-implanted layers, no dislocations were formed for doses as high as $2 \times 10^{16} \text{cm}^{-2}$ after annealing at 1000°C for 1 hour. The threshold was found to be lower for low-energy implantation (100keV): at a dose of $2 \times 10^{16} \text{cm}^{-2}$, when an amorphous layer was formed, microtwins were formed near the projected range upon annealing. Microprecipitates around 50\AA in size were observed in low-energy carbon-implanted samples and the precipitates appeared to be under strain.

Carbon as an impurity in silicon can play an important role in the formation of oxygen precipitates and lattice defects [1-3]. In a recent study, implanted carbon in silicon has been demonstrated to form strong gettering centers for metallic impurities [4-6]. The gettering strength of implanted carbon is close to the gettering strength of noble gas ions and more than ten times higher than those of implanted boron, nitrogen, or oxygen. It has also been reported that dislocations were absent in mega-electron-volt carbon ion implanted layers after one hour annealing at 1000°C, even for doses as high as $2 \times 10^{16} \text{cm}^{-2}$. By comparison, dislocations are commonly observed secondary defects after thermal annealing for boron, phosphorus, and arsenic implantations at even moderate doses (10^{14}cm^{-2} to 10^{15}cm^{-2}). To further explore the behavior of carbon in silicon and its role in crystalline defect formation, we have used cross-section transmission electron microscopy (XTEM) to analyze the carbon-implanted layers under different implantation conditions.

In this experiment, n-type (100) Czochralski (CZ) silicon wafers with resistivity of 3-5 ohm-cm were used as starting material. Both high-energy and low-energy carbon implanted samples were studied. The high-energy implantations were done at 1.9 and 2.4 MeV, while the low-energy implantation was done at 100 keV. The implant doses ranged from 10^{15}cm^{-2} to $2 \times 10^{16} \text{cm}^{-2}$. The implanted wafers were subsequently annealed at 1000°C in N_2 ambient for 1 hour. XTEM analyses were performed on annealed samples to study the defect structures of the carbon implanted layers. In the low-energy implanted samples, channeling analysis with Rutherford backscattering spectrometry (RBS) was also used to assess the amount of lattice disorder before and after annealing.

Figure 1(a) is a XTEM micrograph (bright field) taken from an annealed sample implanted with 1.9 MeV carbon at a dose of $2 \times 10^{15} \text{cm}^{-2}$. The projected range and straggle of carbon ions at 1.9 MeV are 2.2 μm and 0.15 μm respectively, as calculated with the Monte Carlo simulation code TRIM88 [7]. The carbon concentration is around $8 \times 10^{19} \text{cm}^{-3}$ at the peak of the implant profile.

Notice that no extended defects were observed from the surface region down to the depth of the projected range.

Shown in Figure 1(b) is a XTEM micrograph (bright field) of an annealed sample implanted with 2.4MeV carbon at a dose of $2 \times 10^{16} \text{cm}^{-2}$. From TRIM simulation, the projected range and straggle of 2.4MeV carbon ions are $2.6 \mu\text{m}$ and $0.15 \mu\text{m}$ respectively. The corresponding peak concentration of carbon near the projected range is $8 \times 10^{20} \text{cm}^{-3}$, which is equivalent to 1.6 at.%. No dislocations could be observed in this high dose implanted sample either. Instead, a band slightly darker than the silicon matrix with a thickness of about $0.5 \mu\text{m}$ could be seen near the projected range of the C implant profile. Selected area diffraction pattern showed no features different from that of the silicon matrix, indicating that the dark layer is not due to the formation of different phases. The dark band was probably due to a high density of point-defect clusters or microprecipitates in the carbon-rich layer, causing incoherent scattering.

It has been reported that bands of dislocations are produced with the implantation of other ions even at the dose range of 10^{14}cm^{-2} [8,9]. In the case of MeV B or P implantation, a dose of only $5 \times 10^{14} \text{cm}^{-2}$ would create a layer of dislocation loops after a similar annealing treatment. The absence of any extended defects after such high-dose carbon implantation and subsequent annealing is therefore a very surprising phenomenon. One tentative explanation is that the implanted carbon atoms sink the excess Si self-interstitials which are responsible for the dislocation growth and therefore quench the formation of dislocations. Substitutional carbon in silicon is known to shrink local lattice which leaves room for the formation of Si_xC agglomerates and impurity precipitates such as SiO_2 [1-3]. On the other hand, it has been observed that the dislocations produced by ion implantation and subsequent annealing are extrinsic in nature and are probably formed by aggregation of silicon self-interstitials. If the excess self-interstitials are absorbed by the strained carbon-rich layers, dislocation formation can be retarded [8].

In contrast to high-energy deep-implanted layers, both dislocation and precipitate bands are observed in low-energy carbon-implanted layers after annealing. Shown in Figure 2(a)-(c) are XTEM micrographs of samples implanted with 100keV carbon at three different doses and annealed. The projected range and straggle for 100keV carbon in silicon are $0.28\mu\text{m}$ and $0.07\mu\text{m}$ respectively. Figure 2(a) is a XTEM micrograph of a sample implanted at a dose of 10^{15}cm^{-2} . The peak carbon concentration is about $8 \times 10^{19}\text{cm}^{-3}$, similar to the 1.9 MeV implanted sample in Figure 1(a). TRIM simulation indicates that the displacement damage density near the projected ranges in these two cases are also similar. No dislocation formation was observed in the carbon implanted layer.

At doses around 10^{16}cm^{-2} , dislocations and twins can be formed in low-energy carbon implanted layers. Shown in Figure 2(b) is a XTEM micrograph taken from a sample implanted with 100keV carbon at a dose of 10^{16}cm^{-2} , whose peak carbon concentration and damage density are similar to that of the sample shown in Figure 1(b). Both dislocations and small precipitates were formed in this low-energy implanted sample. The dislocation layer is centered around the penetration depth of the carbon implant and has a spread of about $0.1\mu\text{m}$. The precipitates are around 50\AA in size and are distributed in a band of about $0.3\mu\text{m}$. The difference in their distributions suggests that the dislocations are not caused by the precipitates.

The defect structures changed drastically as the implant dose increased from 10^{16}cm^{-2} to $2 \times 10^{16}\text{cm}^{-2}$ at 100keV. Figure 2(c) shows a sample implanted with 100keV carbon at a dose of $2 \times 10^{16}\text{cm}^{-2}$. A layer of extended defects aligned along the $\langle 111 \rangle$ directions is evident from the XTEM micrograph. Shown as the insert is a selected area diffraction pattern taken from an area containing the defect layer. From the diffraction pattern, the defect structure can be identified as twinning. The addition of two spots at $\frac{1}{3}\{111\}$ from every matrix diffraction spot is the fingerprint of $\{111\}$ twinning while the streaking along $\langle 111 \rangle$ is associated with the related stacking faults. The twin-containing layers do not extend to the surface, but are confined to a layer of a

thickness of about 500Å. The silicon above the twin-containing layer is single-crystalline. Besides the microtwins, large number of precipitates of the size about 50Å were found surrounding the twinning layer.

RBS channeling analysis of the low-energy as-implanted samples revealed that an amorphous layer was created with a dose of $2 \times 10^{16} \text{cm}^{-2}$, while the sample with a dose of $1 \times 10^{16} \text{cm}^{-2}$ was not completely amorphized. Figure 3 shows the RBS random and channeling spectra of both samples before annealing. For the sample with a dose of $2 \times 10^{16} \text{cm}^{-2}$ the backscattering signal from the implanted depth reaches the random yield, indicating the existence of a completely amorphized layer. The thickness of the amorphous region is about 1600Å, starting from a depth of about 1200Å. For an implant dose of $1 \times 10^{16} \text{cm}^{-2}$, the damage was not high enough to reach complete amorphization. These observations suggest that the twins were formed during the solid-phase epitaxial growth (SPEG) of the amorphous layer. The high concentration of carbon (around 1 at.%), either in the form of microprecipitates or isolated impurities, disturbed the regular stacking sequence during SPEG and twins were formed. Since the amorphous layer did not extend to the surface, the regrowth fronts proceeded from both the top and bottom amorphous/crystalline interfaces, resulting in a buried layer of microtwins.

The difference between the secondary defects in the low-energy and high-energy implanted cases indicates that the distance to the free surface is an important factor in the formation of dislocations and precipitates in carbon implanted layers. Our previous studies on the gettering of oxygen by carbon implants from CZ silicon substrates indicate that shallower carbon implants getter more oxygen. Using secondary ion mass spectroscopy (SIMS) analysis, for a 2.4 MeV carbon implant with a dose of $2 \times 10^{16} \text{cm}^{-2}$, the gettered oxygen concentration will reach a peak value of $2 \times 10^{18} \text{cm}^{-3}$ after a 1000°C annealing for one hour[5]. In contrast, the gettered oxygen peak concentration in 100keV carbon implanted layers (dose = 10^{16}cm^{-2}) after the same annealing condition can reach 10^{19}cm^{-3} [4]. The larger amount of oxygen gettered by the shallower carbon implant is

probably due to residual oxygen in the annealing nitrogen ambient and can account for the effective nucleation of secondary defects.

The above results are summarized in Table I according to the peak carbon concentration in the samples. At a peak concentration of $8 \times 10^{19} \text{cm}^{-3}$, no extended defects of any kind could be observed in the 1.9MeV and 100 keV implanted samples. At a peak concentration of $8 \times 10^{20} \text{cm}^{-3}$, a band of point-defect clusters or microprecipitates was observed in 2.4MeV carbon implanted layer, while both dislocations and precipitates were found in the 100keV implanted sample. For a high dose at 100keV ($2 \times 10^{16} \text{cm}^{-2}$) which gives a peak carbon concentration of $1.6 \times 10^{21} \text{cm}^{-3}$, an amorphous layer was created after implantation. Precipitates and microtwins were formed near the projected range upon annealing. The precipitates observed in 100keV implanted samples had sizes around 50\AA .

This work was supported in part by California State MICRO program and also supported by the Director, Office of Energy Research, Office of Basic Sciences, Materials Sciences Division, of the U.S. Department of Energy under Contract No. DE-AC03-76SF00098.

References

- [1] U. Gosele, *Mat. Res. Soc. Symp. Proc.* vol. 59, 419 (1986).
- [2] B. O. Kolbesen and A. Muhlaier, *Solid-state Electron.* 25, 759 (1982).
- [3] F. Shimura, *J. Appl. Phys.* 59, 3251 (1986).
- [4] H. Wong, N.W. Cheung, P.K. Chu, *Appl. Phys. Lett.* 52(11), 889 (1988).
- [5] H. Wong, N.W. Cheung, P.K. Chu, J. Liu and J.W. Mayer, *Appl. Phys. Lett.* 52(12), 1023 (1988).
- [6] H. Wong and N. W. Cheung, *Mat. Res. Soc. Symp. Proc.* vol. 147, 97, (1989).
- [7] J. F. Ziegler, J.P. Biersack and U. Littmark, *The Stopping and Range of Ions in Solids*, vol. 1 (Pergamon Press, New York, 1985).
- [8] K. S. Jones, Ph.D dissertation, University of California at Berkeley, (1987).
- [9] M. Tamura, N. Natsuaki, Y. Wada, and E. Mitani, *Nucl. Instrum. and Meth.*, B21, 438 (1987).

Figure Captions

Figure 1. XTEM micrographs (bright field) showing MeV carbon ion implanted layers after annealing at 1000°C for 1 hour. (a) 1.9MeV at a dose of $2 \times 10^{15} \text{cm}^{-2}$, (b) 2.4MeV at a dose of $2 \times 10^{16} \text{cm}^{-2}$. Only the regions around the projected ranges are shown in the micrographs.

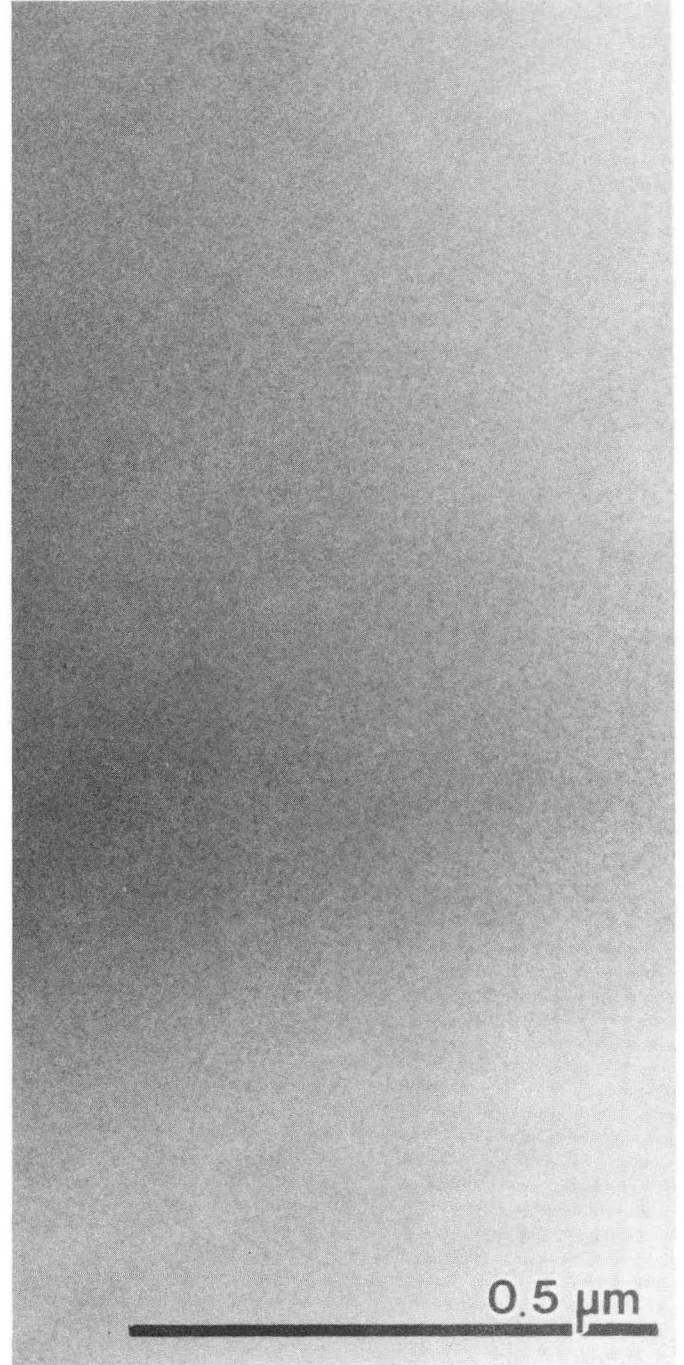
Figure 2. XTEM micrographs (dark field at weak beam condition) showing 100keV carbon implanted layers after annealing at 1000°C for 1 hour. (a) no structural changes were seen for dose = 10^{15}cm^{-2} , (b) dislocations and microprecipitates were visible for dose = 10^{16}cm^{-2} , and (c) both a higher density of dislocations and microtwins were observed for dose = $2 \times 10^{16} \text{cm}^{-2}$. Only the regions around the projected range are shown in the micrographs.

Figure 3. RBS random and channeling spectra measured from 100keV carbon implanted samples before annealing. The implant doses for both samples are: (a) 10^{16}cm^{-2} , (b) $2 \times 10^{16} \text{cm}^{-2}$.

Table I

Summary of the XTEM results. The samples were all annealed at 1000°C for 1 hour in a nitrogen ambient.

Peak Conc. (cm ⁻³)	8×10 ¹⁹	8×10 ²⁰	1.6×10 ²¹
100keV	no extended defects	precipitates + dislocations	precipitates + microtwins
1.9-2.4MeV	no extended defects	precipitates	



XBB 901-740

Figure 1 a,b

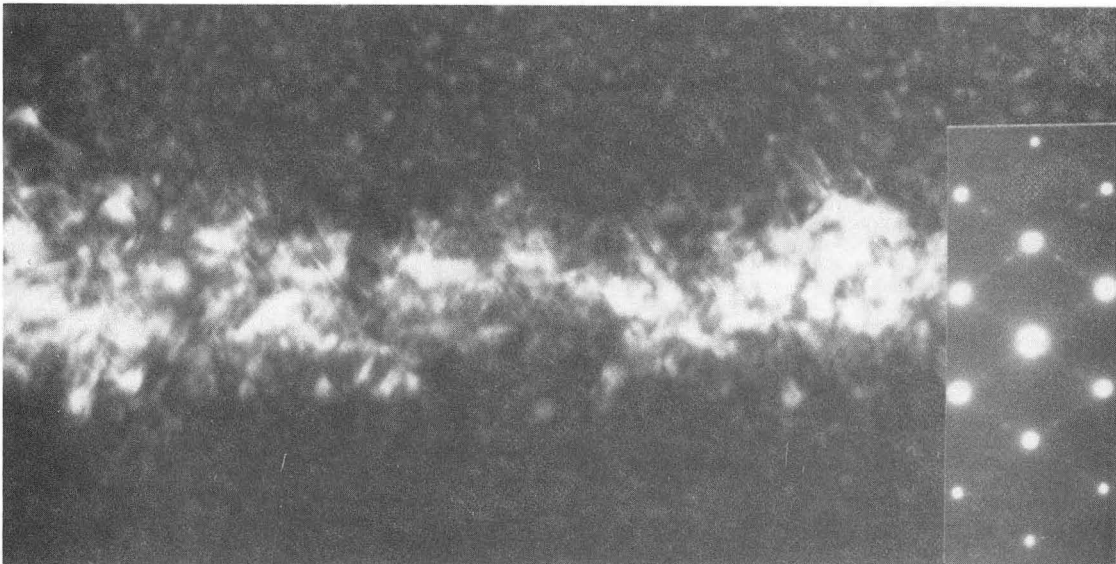
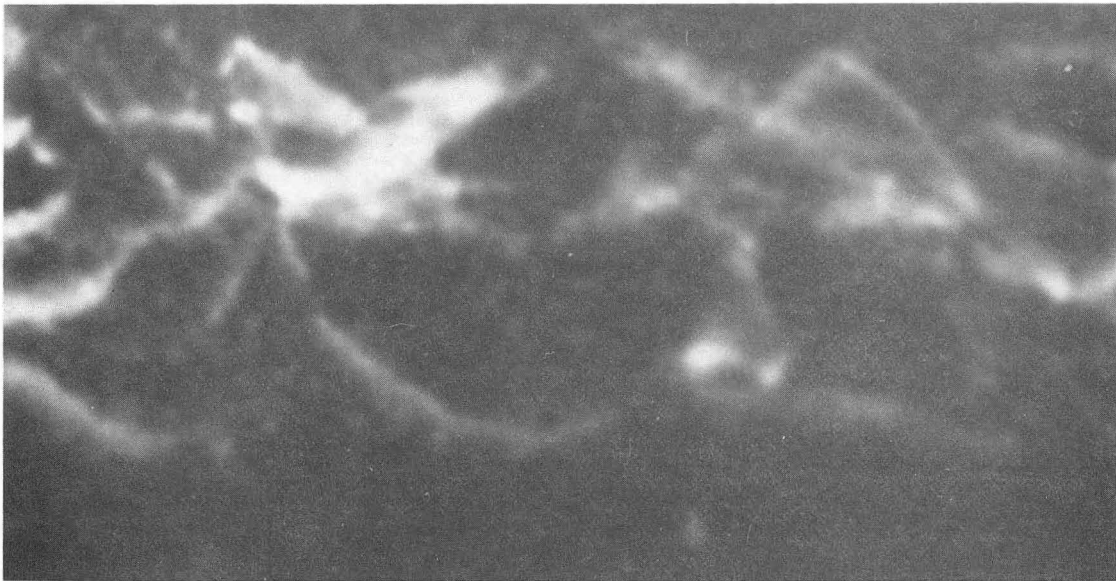
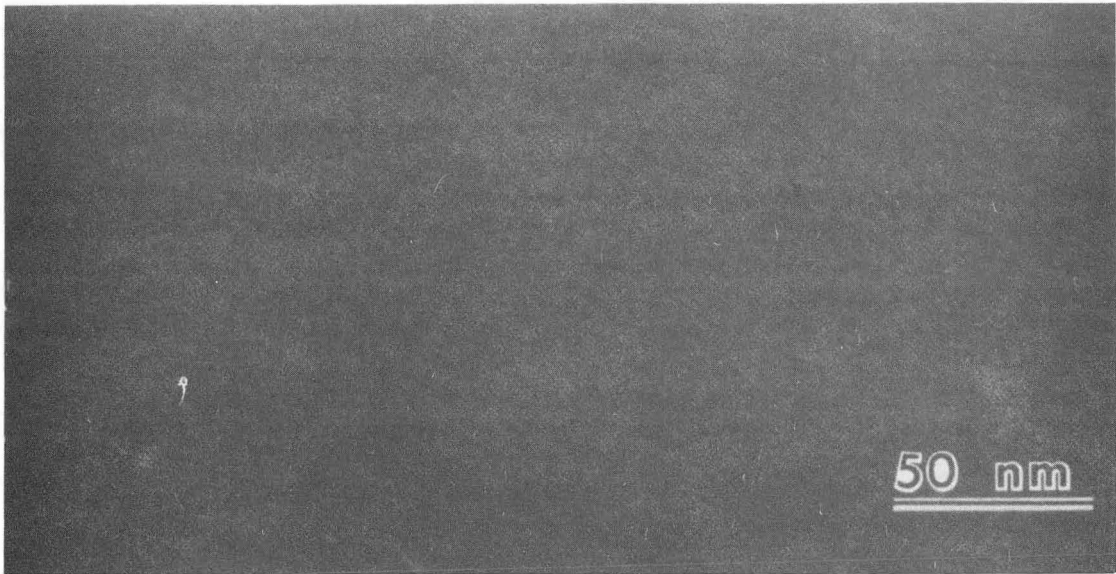
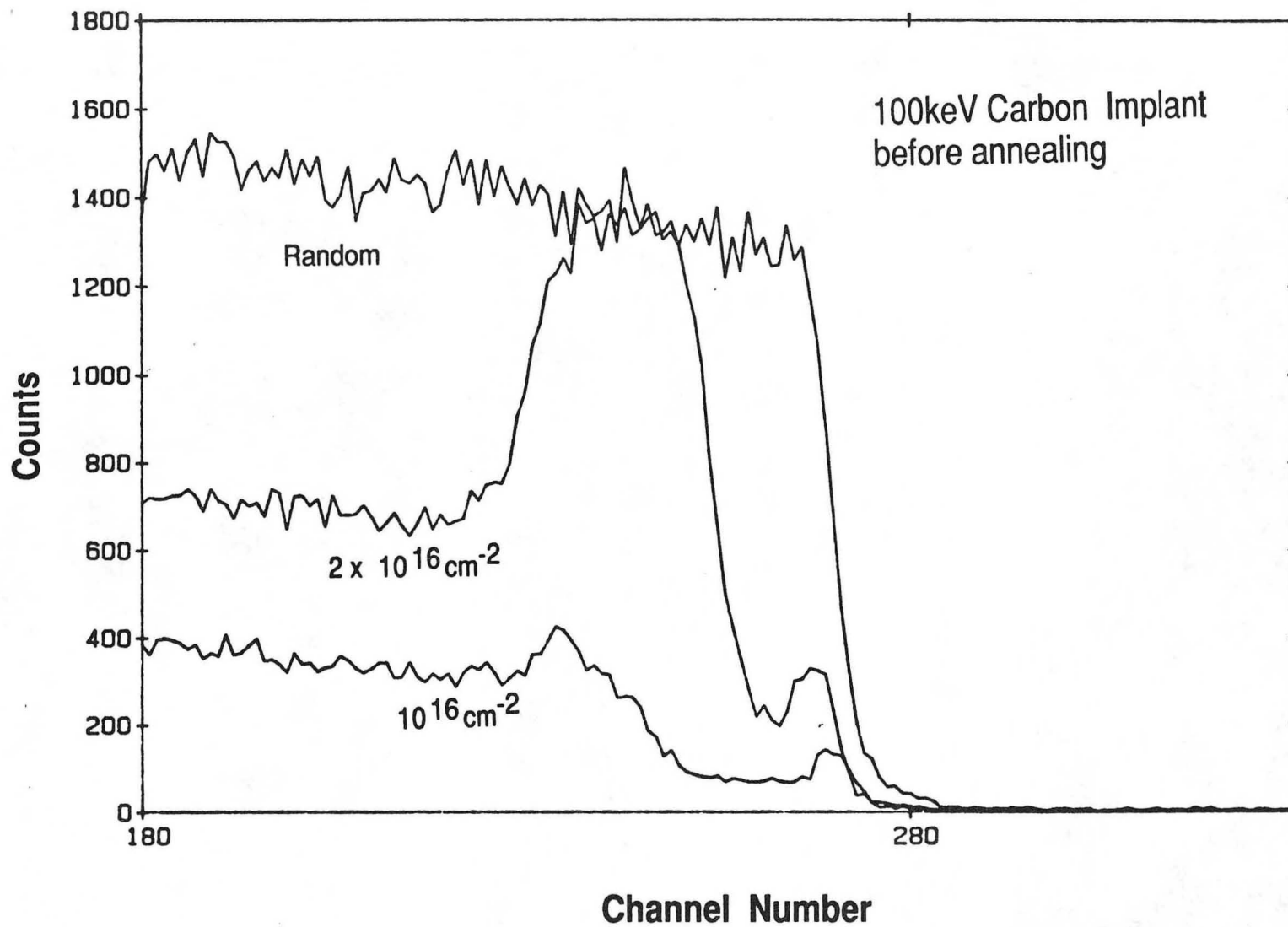


Figure 2 a-c

XBB 901-741



-12-

XBL 901-312

Figure 3

LAWRENCE BERKELEY LABORATORY
UNIVERSITY OF CALIFORNIA
INFORMATION RESOURCES DEPARTMENT
BERKELEY, CALIFORNIA 94720